

# Iterative Soft Shrinkage Learning for Efficient Image Super-Resolution

Jiamian Wang<sup>1\*</sup>, Huan Wang<sup>2</sup>, Yulun Zhang<sup>3</sup>, Yun Fu<sup>2</sup>, and Zhiqiang Tao<sup>1</sup>

<sup>1</sup>Rochester Institute of Technology, <sup>2</sup>Northeastern University, <sup>3</sup>ETH Zürich

## Abstract

The field of image super-resolution (SR) has witnessed extensive neural network designs from CNN to transformer architectures. However, prevailing SR models suffer from prohibitive memory footprint and intensive computations, which limits further deployment on computational-constrained platforms. In this work, we investigate the potential of network pruning for super-resolution to take advantage of off-the-shelf network designs and reduce the underlying computational overhead. Two main challenges remain in applying pruning methods for SR. First, the widely-used filter pruning technique reflects limited granularity and restricted adaptability to diverse network structures. Second, existing pruning methods generally operate upon a pre-trained network for the sparse structure determination, failing to get rid of dense model training in the traditional SR paradigm. To address these challenges, we adopt unstructured pruning with sparse models directly trained from scratch. Specifically, we propose a novel Iterative Soft Shrinkage-Percentage (ISS-P) method by optimizing the sparse structure of a randomly initialized network at each iteration and tweaking unimportant weights with a small amount proportional to the magnitude scale on-the-fly. We observe that the proposed ISS-P could dynamically learn sparse structures adapting to the optimization process and preserve the sparse model's trainability by yielding a more regularized gradient throughput. Experiments on benchmark datasets demonstrate the effectiveness of the proposed ISS-P compared with state-of-the-art methods over diverse network architectures.

## 1. Introduction

Single image super-resolution [15, 17] aims to reconstruct the high-resolution (HR) image from a low-resolution (LR) input. Towards a high-fidelity reconstruction, research efforts have been made by relying on the strong modeling capacity of convolutional neural networks [5, 16, 22, 40]. More recently, advanced Transformer architectures [21, 38, 43] are elaborated, enabling photorealistic retrieval. Despite

the impressive performance, the excessive memory footprint of existing models has been *de facto* in the field, which inevitably prohibits the deployment of advanced SR models on computational-constrained devices.

To alleviate the computational complexity, we study network pruning in this work, which takes advantage of off-the-shelf advanced network architectures to realize efficient yet accurate SR models. Network pruning has been long developed in two mainstream directions. On the one hand, filter pruning (structured pruning) [20] cuts off the specific filter of convolutional layers, among which representative practices in SR is to prune cross-layer filters governed by residual connections [41, 42]. However, these methods need to consider the layer-wise topology by posing structural constraints, requiring a heuristic design and thus making them inflexible. Plus, filter pruning inhibits a more granular manipulation to the network. On the other hand, weight pruning (unstructured pruning) directly removes weight scalars across the network, endowed with more flexibility by accommodating weight discrepancy. Also, the weight pruning method allows a very high pruning ratio, *e.g.*, a ratio of 99% with competitive performance [8, 9]. To this end, this work focuses on delivering a highly-adaptive unstructured pruning solution for diverse SR architectures.

Generally, pruning algorithms are widely recognized to have three steps: (1) pre-training, (2) sparse structure acquisition, and (3) fine-tuning the sparse network. Among these steps, the dense network pre-training usually introduces heavy costs beyond the sparse network optimization. For example, before obtaining a sparse network, the CAT [43] network architecture takes 2 days to train its dense counterpart on 4 A100 GPUs. Thus, a natural question arises to save training time further – can we directly explore the sparsity of network structures from random initialization?

We start from the baseline method by performing random pruning on weights at initialization, whose limitation is the irrelevance between the sparse structure and the weight distribution varying to the optimization. Following this line, we apply the widely-used  $L_1$  norm [20] pruning on randomly initialized weights. However, the immutable sparsity cannot be well aligned with the optimization, leading to limited performance. To tackle this problem, we introduce an

\*Corresponding Author: jw4905@rit.edu

iterative hard thresholding [2, 3] method (IHT) stemming from compressive sensing [4, 6], where the iterative gradient descent step is regularized by a hard thresholding function. Unlike previous works, we tailor IHT to iteratively set unimportant weights as zeros and preserve the important weight magnitudes. By this means, the sparse structure adapts to the weight distribution throughout the training, which potentially better selects essential weights. However, the sparse structure alignment in IHT is heavily susceptible to the magnitude-gradient relationship. The zeroed weight can be continually trapped as “unimportant” once the scales of magnitude and gradient are incomparable. Moreover, by directly zeroing out unimportant weights, IHT blocks the error back-propagation at each iteration, especially hindering the optimization in shallow layers.

To address the aforementioned negative effects, we introduce a more flexible thresholding function for an expressive treatment of unimportant weights. A natural tuning approach is to softly shrink the weights rather than hard threshold. We first explore the soft shrinkage by a growing regularization method [42], namely ISS-R. Per each iteration, the proposed ISS-R constrains weight magnitudes with a gradually increasing weighted  $L_2$  norm, to avoid the conflict between network pruning and smooth sparse network optimization. However, the growing regularization schedule involves a number of hyperparameter tuning, requiring cumbersome manual efforts. Notably, the  $L_2$  regularization shrinkage inside ISS-R is, in essence, proportional to the weight magnitude. Based on this insight, we propose a new iterative soft shrinkage function to simplify the regularization by equivalently shrinking the weight with a percentage (ISS-P). It turns out that ISS-P not only encourages dynamic network sparsity, but also preserves the sparse network trainability, resulting in better convergence. We summarize the contributions of this work as follows:

- We introduce a novel unstructured pruning method, namely iterative soft shrinkage-percentage (ISS-P), which is compatible with diverse SR network designs. Unlike existing pruning strategies for SR, the proposed method trains the sparse network from scratch, providing a practical solution for sparse network acquisition under computational budget constraints.
- We explore pruning behaviors by interpreting the trainability of sparse networks. The proposed ISS-P enjoys a more promising gradient convergence and enables dynamic sparse structures in the training process, offering new insights to design pruning methods for SR.
- Extensive experimental results on benchmark testing datasets at different pruning ratios and scales demonstrate the effectiveness of the proposed method compared with state-of-the-art pruning solutions.

## 2. Related Work

**Single Image Super-Resolution.** The task of single image super-resolution has been developed with remarkable progress since the first convolutional network of SR-CNN [5] was introduced. By taking advantage of the residual structure [10], VDSR [16] further encourages fine-grained reconstruction at rich textured areas. Based on it, EDSR [22] witnessed a promotion by empowering the regression with deeper network depth and a simplified structure. Besides, RCAN [40] outperforms its counterparts by incorporating channel attention into the residual structure. More recently, transformer [7, 33] has become a prevailing option due to its long-range dependency modeling capacity. Among them, SiwnIR [21] equips attention with spatial locality and translation invariance properties. Another design of CAT [43] allows a more flexible window interaction, exploiting the power of the transformer in a novel direction. However, advanced SR models are characterized by rising computational overhead and growing storage costs.

**Neural Network Pruning in SR.** Neural network pruning [28, 31] compresses and accelerates the network by removing redundant parameters. It has been developed in two categories: (1) Structured pruning, which mainly refers to the filter pruning [11, 12, 19, 20, 37], removes the redundant filters for a sparsity pattern exploitation. Recently, two novel works discussed the filter pruning specialized for SR models. ASSL [41] handles the residual network by regularizing the pruned filter locations of different layers upon an alignment penalty. Following ASSL, SRP [42] makes a step further by simplifying the determination of pruned filter indices and yields a state-of-the-art performance. However, both of them require heuristic design for the pruning schema, failing to extend to diverse neural architectures. (2) Unstructured pruning (weight pruning) [9] directly manipulates the weights for the sparsity determination. Despite the flexibility, there lacks an effective pruning strategy proposed to broadly handle advanced SR networks. Our work is to deliver a more generalized solution for different architectures. Besides our setting, another emerging approach is to develop fine-grained pruning upon N:M sparsity [14, 25]. Among them, SLS [26] adapts the layer-wise sparsity level upon trade-off between the computational cost and performance for the convolutional network pruning. Yet, the effectiveness of this method toward novel neural architectures, *e.g.*, Transformers, has not been explored.

## 3. Method

We give the background of SR in Section 3.1 and pruning prerequisites in Section 3.2. We then tailor the classic pruning method to SR by iterative hard thresholding (IHT) in Section 3.3. We develop our method of iterative soft shrinkage by percentage (ISS-P) in Section 3.4.

### 3.1. Single Image Super-resolution

The task of single image super-resolution is to reconstruct the high-resolution (HR) image  $I_{\text{HR}}$  upon the low-resolution (LR) counterpart  $I_{\text{LR}}$  as  $I_{\text{HR}} = F(\Theta; I_{\text{LR}})$ , where  $F(\cdot)$  is the SR network and  $\Theta$  denotes all of the learnable parameters in the network. Given a training dataset  $\mathcal{D}$ , privileging practice is to formulate the SR as a pixel-wise reconstruction problem and solve it with the MSE loss by

$$J(\Theta; \mathcal{D}) = \frac{1}{|\mathcal{D}|} \sum_{\mathcal{D}} \|F(\Theta; I_{\text{LR}}) - I_{\text{HR}}\|^2, \quad (1)$$

where  $I_{\text{LR}}, I_{\text{HR}} \in \mathcal{D}$ . While existing deep SR networks have achieved an impressive photorealistic performance, their cumbersome computation inhibits further deployment on edge devices. In this work, we propose a generalized pruning method for off-the-shelf network designs. We introduce the prerequisites for pruning in the following.

### 3.2. Prerequisites for Pruning

**Pruning Granularity.** Pruning granularity refers to the basic weight group to be removed from the network. In unstructured (weight) pruning, weight scalars are taken as manipulation units, which allows different treatment toward the neighbored weights. Besides, recent SR models have been advanced with diverse operators and structures, *e.g.*, convolution, multi-head self-attention, residual blocks, etc. Unstructured pruning can be flexibly incorporated into diverse structures without additional constraints.

**Pruning Schedule.** The prevailing pruning schedule is widely recognized as three steps: (1) pre-training a dense network, (2) pruning, and (3) fine-tuning the sparse network for performance compensation. However, training a dense SR network in step (1) from scratch already introduces heavy costs beyond the sparse network optimization in step (2~3). To alleviate this problem, in this work, we exploit the sparse network acquisition schedule directly from networks at random initialization and get rid of the first step.

**Baseline Methods.** Bearing with above considerations, we firstly apply several baseline pruning methods to randomly initialized SR networks, including 1) directly training a sparse network with a random sparse structure, namely scratch, and 2)  $L_1$  norm pruning (dubbed as  $L_1$ -norm) [20]. These two baselines, ScTrach and  $L_1$  norm, are widely used in mainstream pruning literature. However, they both fail to adjust the sparse structure adapting to the weight magnitude fluctuation incurred by gradient descent – initially unimportant weights with small magnitude can be finally preserved due to negligible gradient at a certain iterations of backpropagation, while initially important weights (large magnitude) with prominent gradients can be eliminated.

**Notations.** Let  $k \in K$  be the training iterations, where  $K$  is consistent among different pruning methods. Pruning is conducted in a layer-wise manner in each iteration. Given

a network with  $L$  layers, we define  $\theta_l^{[k]} \in \Theta$  as an arbitrary weight magnitude in the  $l$ -th layer at  $k$ -th iteration. Without losing the generality, we will present pruning by taking the  $\theta_l^{[k]}$  as an example throughout the methodology.

### 3.3. Iterative Hard Thresholding

To better capture essential network weights during the optimization, we introduce an iterative hard thresholding (IHT) method in light of compressive sensing (CS) [4, 6]. Typically, IHT operates on the iterative gradient descent with a *hard thresholding* function, serving as a widely-used method for  $L_0$ -norm-based non-convex optimization problems [3]. Unlike the IHT practices in CS, we develop a hard thresholding function  $H(\cdot)$  to adjust the weight magnitudes, which takes effect at the each forward propagation by

$$\theta_l^{[k]} = H(\theta_l^{[k]}) \text{ where } H(\theta_l^{[k]}) = \begin{cases} \theta_l^{[k]}, & \text{if } \theta_l^{[k]} \geq \tau_l^{[k]}, \\ 0, & \text{if } \theta_l^{[k]} < \tau_l^{[k]}, \end{cases} \quad (2)$$

where  $\tau_l^{[k]}$  denotes the threshold magnitude of the  $l$ -th layer at  $k$ -th iteration, determined by an  $L_1$ -norm sorting of the  $l$ -th layer weights with a given pruning ratio  $r$ . We define pruning iterations as  $K_p$ , after which we freeze the sparsity pattern by exchanging  $\tau_l^{[k]}$  with  $\tau_l^{[K_p]}$ , and continually fine-tune the model for another  $K_{\text{FT}}$  iterations for performance compensation. Note that we have  $K = K_p + K_{\text{FT}}$ , where the total training iterations  $K$  equals to the sum of pruning iterations  $K_p$  and the fine-tuning ones  $K_{\text{FT}}$ . There are no modifications to the backpropagation in training.

Different from the static mask determination, the sparse structure of IHT changes during the optimization on-the-fly, which allocates more flexibility for fitting the optimal sparse pattern. However, several limitations still exist. The first is a network throughput blocking effect. Consider the back-propagated errors between hidden layers in a neural network,  $\delta_l = [\Theta_{l+1}^T \delta_{l+1}] \odot \sigma'(\mathbf{z}_l)$ , where  $\delta_l$  presents the error propagated to the  $l$ -th layer,  $\Theta_{l+1}$  denotes the weight matrix of the  $(l+1)$ -th layer, and  $\sigma'(\mathbf{z}_l)$  computes the derivative of the activation  $\sigma(\cdot)$  with the hidden representation  $\mathbf{z}_l$ . Due to the iterative hard thresholding operation  $H(\cdot)$ , there will be a certain amount of weights becomes zero, which further suspends the error transmission to the  $l$ -th layer, and thus hindering the update of shallow weights. Secondly, the sparse structure of the IHT is largely susceptible to the relationship between the weight magnitude and gradient. The zeroed weights are vulnerable to being trapped as the “unimportant” category when the gradient is unexpectedly large, leading to a static sparsity during the training. Additionally, the hard thresholding operator uniformly forces all the unimportant weight to be zeros, neglecting the inherent difference between the magnitudes.

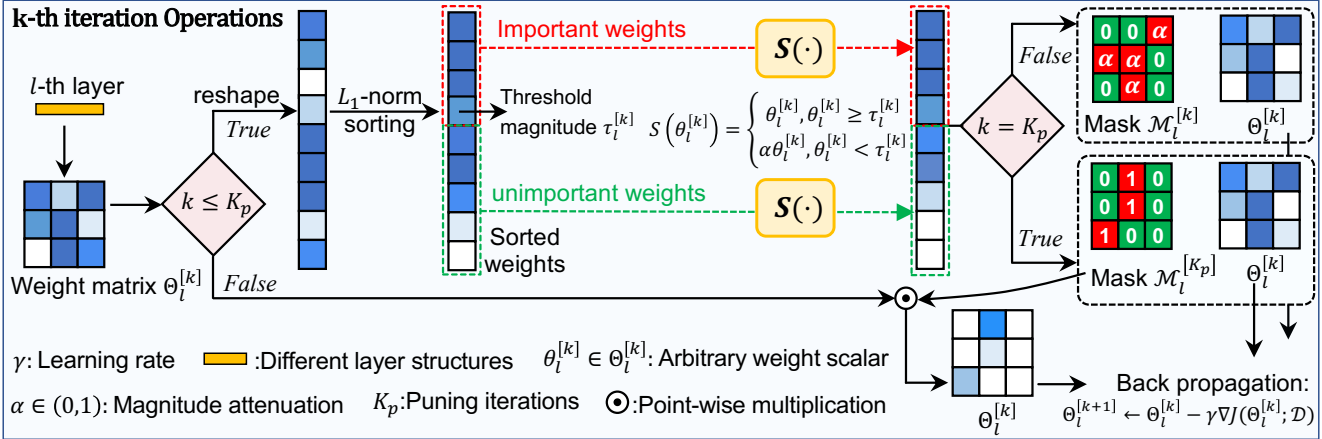


Figure 1. Training pipeline of the proposed Iterative Soft Shrinkage-Percentage (ISS-P), which is exemplified by  $l$ -th learnable layer of the network at  $k$ -th training iteration. In the pruning stage ( $k \leq K_p$ ), ISS-P selectively attenuates the unimportant weight and keeps the essential ones upon  $L_1$ -norm sorting at the forward propagation. In the fine-tuning stage ( $K_p \leq k \leq K_p + K_{FT}$ ), the mask is frozen as  $M_l^{[K_p]}$  and repeatedly applied at each forward propagation. We perform a standard backpropagation in each iteration. The proposed method can flexibly prune different types of layers (*i.e.*, convolution, linear, etc.) and directly trains a sparse network from the random initialization.

### 3.4. Iterative Soft Shrinkage

**Iterative Soft Shrinkage-Regularization (ISS-R).** To address the challenges posed by the IHT, we further tailor the hard thresholding function by offering a more expressive and flexible shrinkage function toward unimportant weights, rather than solely zero-out. Accordingly, we propose a soft shrinkage function  $S(\cdot)$  to facilitate the sparse network training. We first propose a regularization-driven method by introducing an  $L_2$ -norm regularization on weight magnitudes and implement a growing regularization [35] schedule to encourage heterogeneity among unimportant weights, namely iterative soft shrinkage-regularization (ISS-R).

Specifically, given a network with randomly initialized weights, we perform  $L_1$ -norm sorting to the weight magnitudes for the significant weight selection. We then include the unimportant ones into the regularization and impose an  $l_2$  penalty in the backpropagation of each iteration  $k \in K_p$ . Different from IHT, ISS-R naturally integrates the penalization on unimportant weights into optimization. The backpropagation of ISS-R at the pruning stage is given as

$$\theta_l^{[k+1]} \leftarrow \begin{cases} \theta_l^{[k]} - \gamma \nabla J(\theta_l^{[k]}; \mathcal{D}), & \text{if } \theta_l^{[k]} \geq \tau_l^{[k]}, \\ \theta_l^{[k]} - \gamma \nabla J(\theta_l^{[k]}; \mathcal{D}) - 2\eta\theta_l^{[k]}, & \text{if } \theta_l^{[k]} < \tau_l^{[k]}, \end{cases} \quad (3)$$

where  $\gamma$  is the learning rate,  $\eta$  denotes the  $L_2$  regularization penalization scale governed by a gradually growing schedule, *i.e.*,  $\eta = \eta + \delta\eta$  for every  $K_\eta$  iterations, and  $\delta$  controls the growing ratio of  $\eta$ . However, although ISS-R bypasses some limitations of the IHT, it requires tedious hyperparameter tuning (*e.g.*,  $\eta$ ,  $\delta$ ,  $K_\eta$ , etc). Also, it is non-trivial to explain the effect of regularization toward the weight magnitude, leading to a sub-optimal control over the pruning. Therefore, we focus more on annealing weights with magnitude controlling and propose a novel iterative soft shrink-

age by percentage in the following.

**Iterative Soft Shrinkage-Percentage (ISS-P).** Recall that we shrink the weight magnitude with the  $L_2$  regularization in ISS-R, where the penalty intensity is proportional to the weight magnitude (see Eq. (3)). Accordingly, we can achieve the similar ISS effect by directly imposing a percentage function on weights, namely ISS-P. As shown in Fig. 1, the training pipeline of ISS-P can be divided into two stages: 1) pruning and 2) fine-tuning. In the pruning stage, *i.e.*,  $k \leq K_p$ , the weight magnitude of the selected unimportant weights shrinks by a specific ratio. Given the  $l$ -th layer of the network, the soft shrinkage in forward propagation at the  $k$ -th iteration is formulated as

$$\theta_l^{[k]} = m_l^{[k]} \theta_l^{[k]} \text{ where } m_l^{[k]} = \begin{cases} 1, & \text{if } \theta_l^{[k]} \geq \tau_l^{[k]}, \\ \alpha, & \text{if } \theta_l^{[k]} < \tau_l^{[k]}, \end{cases} \quad (4)$$

where we define a mask  $m_l^{[k]} \in \mathcal{M}_l^{[k]}$  accounting for the weight penalization of the layer. The soft shrinkage function can be defined as  $S(\cdot) := m_l^{[k]} \theta_l^{[k]}$ . The  $\alpha \in (0, 1)$  represents the magnitude attenuation, which plays a similar role as the  $\eta$  in ISS-R. The schedule of the  $\alpha$  could be customized by referring to different layers and iterations. In this work, we empirically find that setting  $\alpha$  as a constant value yields a promising performance.

In the fine-tuning stage  $k > K_p$ , we fix the sparse structure and fine-tune the network for the performance compensation, following the same procedure as IHT and ISS-R:

$$\theta_l^{[k]} = m_l^{[K_p]} \theta_l^{[k]} \text{ where } m_l^{[K_p]} = \begin{cases} 1, & \text{if } \theta_l^{[k]} \geq \tau_l^{[k]}, \\ 0, & \text{if } \theta_l^{[k]} < \tau_l^{[k]}, \end{cases} \quad (5)$$

Per each iteration, ISS-P handles the unimportant weight adapting to its magnitude, enabling an intuitive and granular manipulation. Besides, by leveraging a percentage-based soft shrinkage function  $S(\cdot)$ , the sparse network evolves in

---

**Algorithm 1:** ISS-P Training

---

**Input:** train set  $\mathcal{D}$ , initialized parameters  $\Theta$ , pruning ratio  $r$ , total number of learnable layers  $L$ , *i.e.*,  $l \in 1, 2, \dots, L$ . Pruning iterations  $K_p$ , fine tuning iterations  $K_{FT}$ , mask  $\mathcal{M}_l^{[k]} = \emptyset$ , magnitude attenuation  $\alpha$ , learning rate  $\gamma$ ;

**Output:**  $\Theta$

- 1 **for**  $k = 1, \dots, K_p$  **do**
- 2     **for**  $l = 1, 2, \dots, L$  **do**
- 3         Determine the  $\tau_l^{[k]}$  by  $L_1$ -norm sorting;
- 4         Determine the  $\mathcal{M}_l^{[k]}$ ;
- 5         Forward propagation using Eq. (4);
- 6     **end**
- 7     Backpropagation  $\Theta \leftarrow \Theta - \gamma \nabla J(\Theta; \mathcal{D})$  with Eq. (1);
- 8 **end**
- 9 **for**  $k = K_p + 1, K_p + 2, \dots, K_p + K_{FT}$  **do**
- 10    **for**  $l = 1, 2, \dots, L$  **do**
- 11         Forward propagation using Eq. (5);
- 12     **end**
- 13     Backpropagation  $\Theta \leftarrow \Theta - \gamma \nabla J(\Theta; \mathcal{D})$  with Eq. (1);
- 14 **end**

---

a more active way, which substantially explores more sparsity possibilities throughout the optimization. Fig. 2 demonstrates this point by comparing the mask dynamics of ISS-P and IHT in the pruning stage, where we count the permille (%) of the flips between the important/unimportant magnitudes in  $\mathcal{M}_l^{[k]}$ , given by two representative layers of the Transformer backbone SwinIR [21], *i.e.*, 13-th layer and 44-th layer. It can be seen that in each iteration, the number of flips counted on the IHT is quite small, and in most situations, are actually zeros. A lot more flips observed in the training process of ISS-P, *e.g.*, in the 13-th layer, flips that over 0.5% of the total number of the weights are observed during the optimization. Thereby, the sparse structure of IHT remains static in most situations yet that in ISS-P moderately changes, which allows a higher possibility to evade inferior sparse structures. Besides a more dynamical sparsity, the empirical evidence (see Section 4.2) showcases that the proposed ISS-P realizes a more favorable trainability [29, 34] for the sparse network, which indicates a easier convergence for the selected sparse network. The training process of the ISS-P is summarized in Algorithm 1.

## 4. Experiment

**Datasets and Backbones.** Following the recent works [41, 42], we use DIV2K [32] and Flickr2K [22] as the training datasets. Five benchmark datasets are employed for the quantitative comparison and visualization, including Set5 [1], Set14 [39], B100 [23], Urban100 [13], and Manga109 [24]. We adopt PSNR and SSIM [36] as eval-

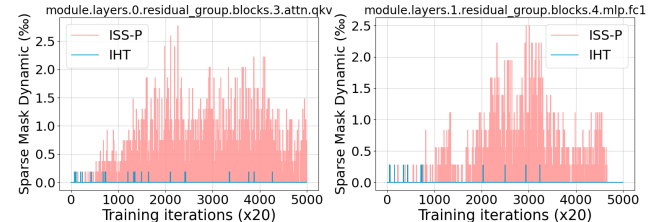


Figure 2. Sparsity dynamics comparison between the ISS-P and IHT in the pruning stage. The proposed method allows a more active sparse pattern exploitation adapting to the optimization. We choose two representative layers from the SwinIR [21] backbone.

uation metrics by referring Y channels in the YCbCr space.

We train and evaluate the proposed method on representative backbones that covering convolutional network and transformer architectures: (1) SwinIR-Lightweight [21], which takes a sub-pixel convolutional layer [30] for the un-sampling and a convolutional layer for the final reconstruction. (2) EDSR-L [22] that consists of 32 residual blocks. (3) Cross-aggregation transformer [43] with regular rectangle window (CAT-R). We prune all of the learnable layers of the corresponding backbones from random initialization.

**Implementation Details.** We conduct the same augmentation procedure as previous works [41, 42] by implementing random rotation of  $90^\circ$ ,  $180^\circ$ ,  $270^\circ$ , and horizontal flip. For network training, we adopt the image patches of  $64 \times 64$  with batch size of 32. For computational efficiency, we set the batch size as 16 for ablation study. The training is performed upon an Adam [18] optimizer with  $\beta_1=0.9$ ,  $\beta_2=0.999$ , and  $\epsilon=10^{-8}$ . The initial learning rate is  $2 \times 10^{-4}$  with a half annealing upon every  $2.5 \times 10^5$  iterations. We empirically determine the magnitude attenuation as  $\alpha=0.95$ . We set the total training iterations as  $K=5 \times 10^5$  for benchmark comparison and  $3 \times 10^5$  for ablation. The pruning stage is  $K_p=1 \times 10^5$ . We implement the proposed method in PyTorch [27] on an NVIDIA RTX3090 GPU.

**Compared Methods.** We compare the proposed method with the classic baseline methods, *i.e.*, training from scratch (dubbed as ‘‘Scratch’’) and  $L_1$ -norm pruning [20] (denoted as ‘‘ $L_1$ -norm’’), as well as the most recent pruning practices [41, 42] dedicated to SR models. All the methods are elaborated under the unstructured pruning, and we have no pre-trained dense networks at the beginning. For the fairness of the comparison, we facilitate the same backbone structure, training iterations, neural network initialization, and pruning ratios for different methods. Among them, ASSL [41] and SRP [42] are developed to remove the filters, but both are readily extendable to unstructured pruning.<sup>1</sup> We keep the pruning constraints of both methods when operating on different backbones. For the proposed method, we use ISS-P as our final pruning treatment owing to its vigorous sparsity dynamics and promising performance.

<sup>1</sup>More details could be found in supplementary.

| Methods          | Scale      | Set5  |        | Set14 |        | B100  |        | Urban100 |        | Manga109 |        |
|------------------|------------|-------|--------|-------|--------|-------|--------|----------|--------|----------|--------|
|                  |            | PSNR  | SSIM   | PSNR  | SSIM   | PSNR  | SSIM   | PSNR     | SSIM   | PSNR     | SSIM   |
| scratch          | $\times 2$ | 37.62 | 0.9591 | 33.16 | 0.9141 | 31.89 | 0.8958 | 30.83    | 0.9142 | 37.69    | 0.9747 |
| $L_1$ -norm [20] | $\times 2$ | 37.62 | 0.9591 | 33.14 | 0.9145 | 31.90 | 0.8960 | 30.90    | 0.9151 | 37.77    | 0.9749 |
| ASSL[41]         | $\times 2$ | 37.69 | 0.9593 | 33.17 | 0.9145 | 31.93 | 0.8964 | 30.96    | 0.9160 | 37.83    | 0.9751 |
| SRP[42]          | $\times 2$ | 37.66 | 0.9592 | 33.20 | 0.9149 | 31.94 | 0.8964 | 31.01    | 0.9165 | 37.88    | 0.9751 |
| ISS-P (ours)     | $\times 2$ | 37.66 | 0.9593 | 33.22 | 0.9146 | 31.93 | 0.8963 | 31.06    | 0.9169 | 37.93    | 0.9753 |
| scratch          | $\times 3$ | 33.72 | 0.9210 | 29.90 | 0.8342 | 28.78 | 0.7971 | 27.06    | 0.8264 | 32.22    | 0.9329 |
| $L_1$ -norm [20] | $\times 3$ | 33.71 | 0.9209 | 29.93 | 0.8344 | 28.79 | 0.7971 | 27.07    | 0.8266 | 32.21    | 0.9331 |
| ASSL[41]         | $\times 3$ | 33.89 | 0.9223 | 30.00 | 0.8355 | 28.42 | 0.7985 | 27.20    | 0.8305 | 32.44    | 0.9355 |
| SRP[42]          | $\times 3$ | 33.86 | 0.9222 | 29.98 | 0.8353 | 28.82 | 0.7980 | 27.19    | 0.8296 | 32.40    | 0.9347 |
| ISS-P (ours)     | $\times 3$ | 33.85 | 0.9224 | 30.00 | 0.8358 | 28.84 | 0.7984 | 27.26    | 0.8313 | 32.48    | 0.9356 |
| scratch          | $\times 4$ | 31.41 | 0.8821 | 28.11 | 0.7700 | 27.25 | 0.7255 | 25.16    | 0.7530 | 28.96    | 0.8847 |
| $L_1$ -norm [20] | $\times 4$ | 31.43 | 0.8822 | 28.12 | 0.7700 | 27.26 | 0.7256 | 25.16    | 0.7530 | 28.96    | 0.8849 |
| ASSL[41]         | $\times 4$ | 31.50 | 0.8841 | 28.19 | 0.7718 | 27.31 | 0.7280 | 25.26    | 0.7583 | 29.20    | 0.8895 |
| SRP[42]          | $\times 4$ | 31.46 | 0.8833 | 28.17 | 0.7713 | 27.29 | 0.7269 | 25.25    | 0.7568 | 29.15    | 0.8879 |
| ISS-P (ours)     | $\times 4$ | 31.60 | 0.8851 | 28.23 | 0.7724 | 27.32 | 0.7277 | 25.32    | 0.7593 | 29.28    | 0.8904 |

Table 1. PSNR/SSIM comparison of the state-of-the-art methods under the pruning ratio of 0.9.

| Methods          | Scale      | Set5  |        | Set14 |        | B100  |        | Urban100 |        | Manga109 |        |
|------------------|------------|-------|--------|-------|--------|-------|--------|----------|--------|----------|--------|
|                  |            | PSNR  | SSIM   | PSNR  | SSIM   | PSNR  | SSIM   | PSNR     | SSIM   | PSNR     | SSIM   |
| scratch          | $\times 2$ | 37.27 | 0.9575 | 32.83 | 0.9106 | 31.63 | 0.8923 | 30.04    | 0.9040 | 36.95    | 0.9720 |
| $L_1$ -norm [20] | $\times 2$ | 37.26 | 0.9574 | 32.83 | 0.9107 | 31.63 | 0.8924 | 30.07    | 0.9044 | 36.95    | 0.9721 |
| ASSL[41]         | $\times 2$ | 37.39 | 0.9581 | 32.92 | 0.9119 | 31.73 | 0.8940 | 30.29    | 0.9080 | 37.21    | 0.9732 |
| SRP[42]          | $\times 2$ | 37.41 | 0.9582 | 32.96 | 0.9124 | 31.75 | 0.8941 | 30.40    | 0.9091 | 37.32    | 0.9734 |
| ISS-P (ours)     | $\times 2$ | 37.46 | 0.9584 | 33.01 | 0.9129 | 31.78 | 0.8945 | 30.52    | 0.9105 | 37.43    | 0.9738 |
| scratch          | $\times 3$ | 33.13 | 0.9144 | 29.52 | 0.8264 | 28.52 | 0.7899 | 26.40    | 0.8075 | 30.98    | 0.9199 |
| $L_1$ -norm [20] | $\times 3$ | 33.14 | 0.9144 | 29.51 | 0.8263 | 28.52 | 0.7899 | 26.39    | 0.8074 | 30.97    | 0.9198 |
| ASSL[41]         | $\times 3$ | 33.37 | 0.9172 | 29.64 | 0.8292 | 28.62 | 0.7932 | 26.61    | 0.8148 | 31.43    | 0.9254 |
| SRP[42]          | $\times 3$ | 33.33 | 0.9167 | 29.65 | 0.8290 | 28.61 | 0.7924 | 26.59    | 0.8131 | 31.36    | 0.9241 |
| ISS-P (ours)     | $\times 3$ | 33.49 | 0.9185 | 29.73 | 0.8306 | 28.66 | 0.7939 | 26.75    | 0.8182 | 31.68    | 0.9277 |
| scratch          | $\times 4$ | 30.70 | 0.8679 | 27.64 | 0.7581 | 26.98 | 0.7154 | 24.56    | 0.7285 | 27.66    | 0.8590 |
| $L_1$ -norm [20] | $\times 4$ | 30.71 | 0.8680 | 27.64 | 0.7580 | 26.98 | 0.7154 | 24.57    | 0.7286 | 27.66    | 0.8590 |
| ASSL[41]         | $\times 4$ | 31.03 | 0.8748 | 27.83 | 0.7628 | 27.09 | 0.7195 | 24.76    | 0.7373 | 28.16    | 0.8701 |
| SRP[42]          | $\times 4$ | 30.99 | 0.8741 | 27.83 | 0.7626 | 27.09 | 0.7193 | 24.79    | 0.7374 | 28.15    | 0.8687 |
| ISS-P (ours)     | $\times 4$ | 31.16 | 0.8775 | 27.93 | 0.7655 | 27.14 | 0.7218 | 24.91    | 0.7436 | 28.44    | 0.8755 |

Table 2. PSNR/SSIM comparison of the state-of-the-art methods under the pruning ratio of 0.95.

#### 4.1. Comparison with Advanced Pruning Methods

**Performance Comparisons.** We conduct a thorough quantitative comparison with different pruning ratios, *i.e.*, 0.9, 0.95, and 0.99, under the scale of  $\times 2$ ,  $\times 3$ , and  $\times 4$ . As shown in Table 1~3, the proposed ISS-P presents a promising performance by improving excising methods with a considerable margin. Notably, the advantage of the ISS-P is amplified when the scale or pruning ratio raises. Thanks to the dedicated design of ISS-P, a more regularized gradient flow is preserved, leading to better trainability, especially for sparse networks with higher scale or pruning ratios. We also provide more analysis on convergence in Section 4.2.

**Visual Comparisons.** We further visually compare the performance of the sparse networks trained with different pruning methods. In Fig. 3~3, we present the results at a challenging scale setting (*i.e.*,  $\times 4$ ) and very high pruning ratio (*i.e.*, 0.99). By comparison, the proposed ISS-P allows a

more granular reconstruction, especially at textured areas with detailed visual ingredients, for example, the arch of the church. Besides, the proposed method produces fewer distortions for regions with high gradients, *e.g.*, by producing clearer and more consistent edges. These observations indicate a better modeling capacity, owing to an appropriate sparse architecture upon active sparse dynamics of ISS-P and a more promising optimization.

**Different Backbones.** In Table 4, we present the effectiveness of the proposed pruning method on different backbones. The ISS-P works favorably well by outperforming baseline and prevailing methods for SR, which is consistent with the results on SwinIR-Lightweight. Results on these backbones demonstrate that the proposed method is network structure-independent, which potentially eases the deployment of advanced SR networks and is actually an important property in practice.

| Methods          | Scale      | Set5  |        | Set14 |        | B100  |        | Urban100 |        | Manga109 |        |
|------------------|------------|-------|--------|-------|--------|-------|--------|----------|--------|----------|--------|
|                  |            | PSNR  | SSIM   | PSNR  | SSIM   | PSNR  | SSIM   | PSNR     | SSIM   | PSNR     | SSIM   |
| scratch          | $\times 2$ | 35.34 | 0.9461 | 31.61 | 0.8988 | 30.65 | 0.8788 | 28.06    | 0.8722 | 32.22    | 0.9536 |
| $L_1$ -norm [20] | $\times 2$ | 35.33 | 0.9460 | 31.61 | 0.8988 | 30.65 | 0.8789 | 28.06    | 0.8722 | 33.21    | 0.9536 |
| ASSL[41]         | $\times 2$ | 35.65 | 0.9486 | 31.82 | 0.9007 | 30.80 | 0.8808 | 28.30    | 0.8760 | 33.83    | 0.9571 |
| SRP[42]          | $\times 2$ | 35.47 | 0.9468 | 31.65 | 0.8992 | 30.70 | 0.8795 | 28.15    | 0.8733 | 33.56    | 0.9551 |
| ISS-P (ours)     | $\times 2$ | 36.36 | 0.9526 | 32.19 | 0.9047 | 31.13 | 0.8853 | 28.89    | 0.8864 | 35.13    | 0.9640 |
| scratch          | $\times 3$ | 31.21 | 0.8822 | 28.27 | 0.8001 | 27.70 | 0.7670 | 25.01    | 0.7600 | 27.85    | 0.8690 |
| $L_1$ -norm [20] | $\times 3$ | 31.21 | 0.8821 | 28.27 | 0.8001 | 27.70 | 0.7669 | 25.01    | 0.7600 | 27.85    | 0.8690 |
| ASSL[41]         | $\times 3$ | 31.73 | 0.8928 | 28.62 | 0.8082 | 27.90 | 0.7733 | 25.29    | 0.7710 | 28.54    | 0.8847 |
| SRP[42]          | $\times 3$ | 31.02 | 0.8779 | 28.17 | 0.7968 | 27.65 | 0.7644 | 24.94    | 0.7567 | 27.67    | 0.8630 |
| ISS-P (ours)     | $\times 3$ | 32.07 | 0.8990 | 28.86 | 0.8133 | 28.06 | 0.7774 | 25.54    | 0.7793 | 29.05    | 0.8932 |
| scratch          | $\times 4$ | 29.00 | 0.8197 | 26.48 | 0.7219 | 26.29 | 0.6882 | 23.51    | 0.6769 | 25.43    | 0.7924 |
| $L_1$ -norm [20] | $\times 4$ | 29.00 | 0.8198 | 26.48 | 0.7219 | 26.29 | 0.6882 | 23.51    | 0.6769 | 25.42    | 0.7924 |
| ASSL[41]         | $\times 4$ | 29.15 | 0.8257 | 26.58 | 0.7266 | 26.35 | 0.6917 | 23.58    | 0.6812 | 25.58    | 0.7998 |
| SRP[42]          | $\times 4$ | 28.78 | 0.8120 | 26.33 | 0.7147 | 26.21 | 0.6834 | 23.43    | 0.6713 | 25.18    | 0.7808 |
| ISS-P (ours)     | $\times 4$ | 29.67 | 0.8419 | 26.94 | 0.7373 | 26.55 | 0.6988 | 23.87    | 0.6951 | 26.21    | 0.8205 |

Table 3. PSNR/SSIM comparison of the state-of-the-art methods under the pruning ratio of 0.99.

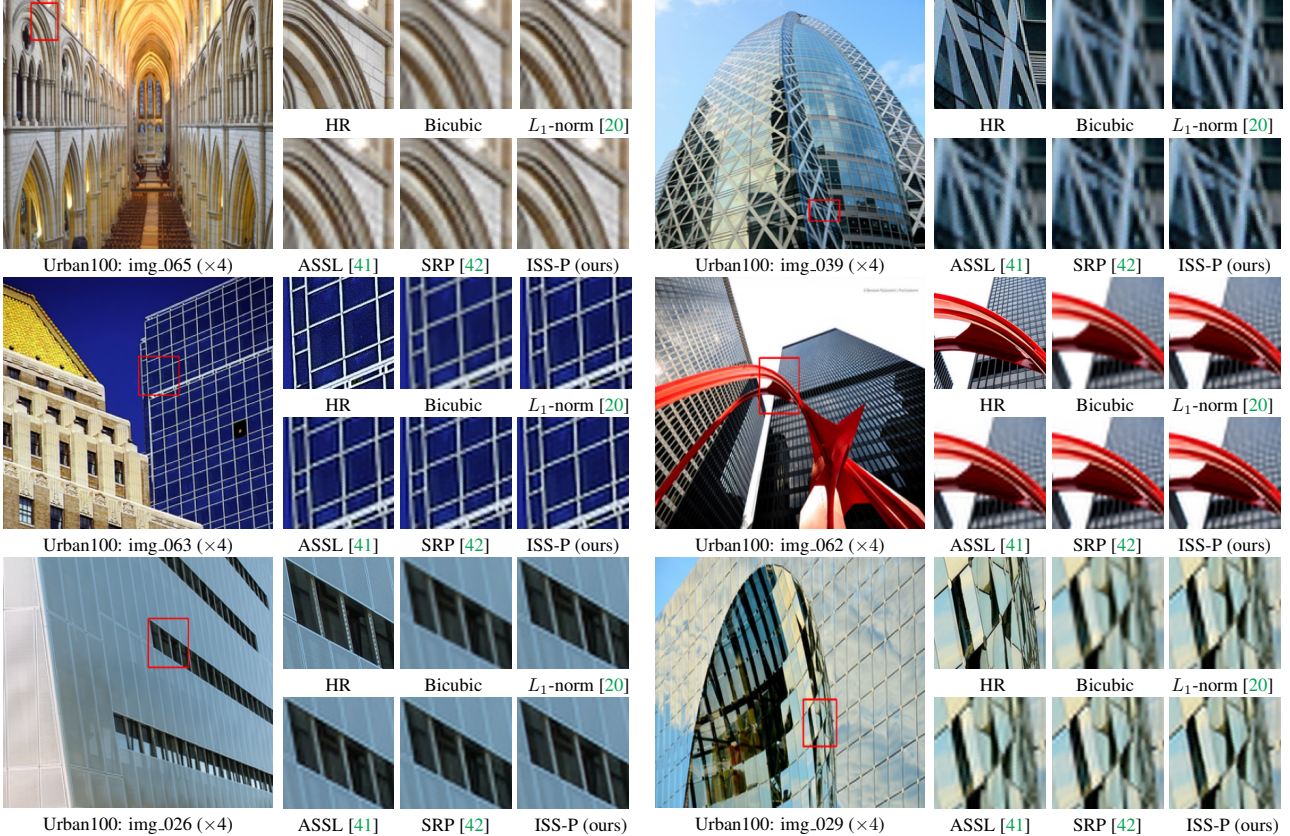


Figure 3. Visualization comparison of different pruning methods on Urban100 [13] dataset.

## 4.2. ISS Analysis

**Ablation Study.** We perform ablation studies of the proposed method under the pruning ratio of 0.9 at different scales. We specifically compare three ablated pruning methods, *i.e.*, IHT, ISS-R, and ISS-P, which explore dynamic sparse structures with different weight annealing operators at each forward propagation procedure. The SwinIR-

Lightweight [21] is adopted as the backbone. As shown in Table 5, the ISS-P consistently outperforms on different testing datasets. For example, the performance gap between ISS-P and ISS-R remains over 0.2dB under the scale of  $\times 4$ . Note that ISS-R is inferior to the IHT at  $\times 2$  scale but surpasses it at the  $\times 4$ . This suggests a strong resilience of ISS-R schedule in trainability preserving albeit a sub-optimal hyperparameter configuration in the growing regularization.

| Backbones | Methods         | Set5  |        | Set14 |        | B100  |        | Urban100 |        | Manga109 |        |
|-----------|-----------------|-------|--------|-------|--------|-------|--------|----------|--------|----------|--------|
|           |                 | PSNR  | SSIM   | PSNR  | SSIM   | PSNR  | SSIM   | PSNR     | SSIM   | PSNR     | SSIM   |
| EDSR-L    | scratch         | 29.60 | 0.8522 | 26.35 | 0.7312 | 25.92 | 0.7003 | 23.69    | 0.7303 | 27.28    | 0.8570 |
|           | $L_1$ norm [20] | 29.61 | 0.8526 | 26.36 | 0.7318 | 25.93 | 0.7011 | 23.70    | 0.7313 | 27.35    | 0.8582 |
|           | ASSL [41]       | 29.85 | 0.8568 | 26.54 | 0.7368 | 26.07 | 0.7064 | 24.09    | 0.7461 | 27.93    | 0.8690 |
|           | SRP [42]        | 29.78 | 0.8558 | 26.47 | 0.7349 | 26.00 | 0.7036 | 23.89    | 0.7392 | 27.72    | 0.8656 |
|           | ISS-P (ours)    | 30.23 | 0.8628 | 26.74 | 0.7428 | 26.21 | 0.7109 | 24.43    | 0.7596 | 28.51    | 0.8783 |
| CAT-R     | scratch         | 32.19 | 0.8940 | 28.61 | 0.7816 | 27.58 | 0.7367 | 26.03    | 0.7846 | 30.50    | 0.8902 |
|           | $L_1$ norm [20] | 32.19 | 0.8940 | 28.59 | 0.7814 | 27.58 | 0.7368 | 26.01    | 0.7842 | 30.52    | 0.9083 |
|           | ASSL [41]       | 32.08 | 0.8930 | 28.53 | 0.7803 | 27.54 | 0.7356 | 25.90    | 0.7809 | 30.35    | 0.9059 |
|           | SRP [42]        | 32.24 | 0.8950 | 28.61 | 0.7827 | 27.60 | 0.7382 | 26.09    | 0.7871 | 30.61    | 0.9096 |
|           | ISS-P (ours)    | 32.66 | 0.9008 | 28.93 | 0.7900 | 27.80 | 0.7444 | 26.94    | 0.8118 | 31.52    | 0.9197 |

Table 4. Performance comparison of different methods upon the representative CNN backbone, EDSR-L [22], and advanced transformer backbone, CAT-R [43], at the scale of the  $\times 4$ . The pruning ratio is 0.95.

| Methods | Scale      | Set5  |        | Set14 |        | B100  |        | Urban100 |        | Manga109 |        |
|---------|------------|-------|--------|-------|--------|-------|--------|----------|--------|----------|--------|
|         |            | PSNR  | SSIM   | PSNR  | SSIM   | PSNR  | SSIM   | PSNR     | SSIM   | PSNR     | SSIM   |
| IHT     | $\times 2$ | 37.48 | 0.9585 | 33.01 | 0.9131 | 31.78 | 0.8947 | 30.56    | 0.9112 | 37.42    | 0.9738 |
| ISS-R   | $\times 2$ | 37.38 | 0.9581 | 32.97 | 0.9121 | 31.72 | 0.8939 | 30.33    | 0.9082 | 37.16    | 0.9730 |
| ISS-P   | $\times 2$ | 37.51 | 0.9587 | 33.05 | 0.9134 | 31.82 | 0.8952 | 30.68    | 0.9125 | 37.54    | 0.9741 |
| IHT     | $\times 3$ | 37.04 | 0.9563 | 32.64 | 0.9091 | 31.49 | 0.8904 | 29.72    | 0.8998 | 36.47    | 0.9700 |
| ISS-R   | $\times 3$ | 37.07 | 0.9566 | 32.66 | 0.9092 | 31.50 | 0.8906 | 29.70    | 0.8995 | 36.51    | 0.9704 |
| ISS-P   | $\times 3$ | 37.31 | 0.9578 | 32.84 | 0.9112 | 31.66 | 0.8929 | 30.14    | 0.9059 | 37.00    | 0.9723 |
| IHT     | $\times 4$ | 35.17 | 0.9448 | 31.49 | 0.8978 | 30.57 | 0.8781 | 27.95    | 0.8740 | 32.91    | 0.9519 |
| ISS-R   | $\times 4$ | 35.37 | 0.9462 | 31.60 | 0.8983 | 30.66 | 0.8790 | 28.10    | 0.8730 | 33.31    | 0.9543 |
| ISS-P   | $\times 4$ | 35.86 | 0.9496 | 31.89 | 0.9015 | 30.87 | 0.8819 | 28.40    | 0.8777 | 34.09    | 0.9584 |

Table 5. Ablation study of different methods under the pruning ratio of 0.9 at different scales.

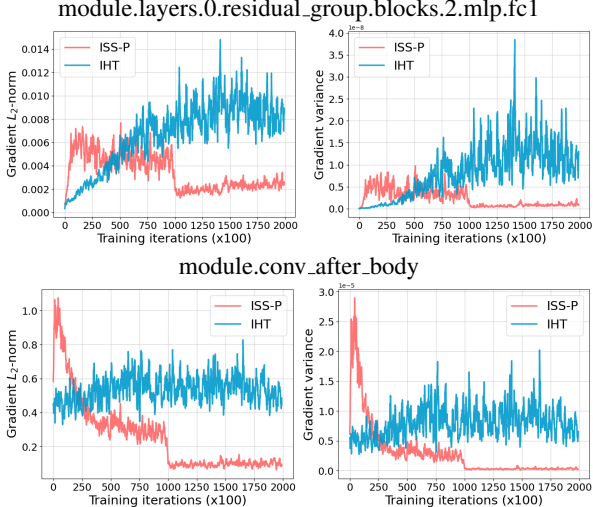


Figure 4. Trainability comparison of the IHT and ISS-P. The layer-wise gradient  $L_2$ -norm and variance in the pruning stage ( $1 \times 10^5$  iterations) and the first  $1 \times 10^5$  iterations of fine-tuning stage are plotted. We choose two representative layers, *i.e.*, a fully connected layer (*top*) and a convolution (*bottom*) from the SwinIR.

**Trainability Analysis.** Trainability depicts whether a network is easy to be optimized, which is highly associated to the sparse structures in the field of pruning. We find that ISS-P better preserves the trainability of the network. Intuitively, this is because the ISS-P better retains the network dynamical isometry [29] by better preserving the weight connections (dependencies) during the training, compared

with IHT. We verify this point by observing the gradient  $L_2$ -norm and variance during the training. In Fig. 4, we find that the gradient norm of the ISS-P steadily converges in the pruning stage ( $K_p < 1 \times 10^5$ ), so that the selected sparse network (taking effect at  $K_p = 1 \times 10^5$ ) approaches the local minimum on the loss landscape at the end. Reversely, the gradient descent of IHT is still ongoing (*i.e.*, iteration  $k = 2 \times 10^5$ ), which indicates the network is harder to converge. A similar conclusion is also validated by comparing more regularized gradient variances of ISS-P against larger gradient variances of IHT. In addition, ISS-P allows better trainability throughout the network, regardless of the depth and layer types, as exemplified by a shallow fully connected layer (11-th) and a deep convolutional layer (101-th).

## 5. Conclusion

In this work, we have studied the problem of efficient image super-resolution by the unstructured pruning treatment upon the network with randomly initialized weights. Specifically, we have proposed an Iterative Soft Shrinkage-Percentage (ISS-P) method to iteratively shrink the weight with a small amount proportional to the magnitude, which has not only enabled a more dynamic sparse structure exploitation but also better retained the trainability of the network. The proposed method has been readily compatible with the off-the-shelf SR network designs, facilitating the sparse network acquisition and deployment.

## Appendix

### A. Overview

In this supplementary material, we present additional results and analyses about the proposed method as follows.

- A more detailed and comprehensive illustration to the performance comparison (Section B).
- Ablation studies under high pruning ratios (Section C).
- More visualization comparisons (Section D).
- More discussions about the dynamics of the sparse structure and trainability preserving (Section E).

### B. Compared Methods

**ASSL.** ASSL [41] prunes the filters of the convolutional layers across different residual blocks, which cannot be easily extended to the novel structures, *e.g.*, multi-layer perceptron, multi-head self-attention, etc. To improve the adaptability of ASSL, we implement this method in a weight pruning fashion by following their designing principles.

Firstly, ASSL selects the last convolutional layers of all residual blocks as *constrained* layers, whose pruned filter indexes should be kept the same across the whole network for the residual connection concern. All the other convolutional layers can be pruned without structural constrains, which are termed as *free* layers. Similarly, we retain this structural constraint by categorizing the learnable layers before the any residual connection as the *constrained* ones, whose pruned wight indexes are consistent to one another, while others are *free* layers without structural constrains.

To select the pruned filter indexes in the *constrained* layers, ASSL firstly employs the weight normalization [?] as an indicator of the filter importance, which in our case, can be directly inferred from the weight magnitudes. Thereby, no additional weight normalization is needed in our setting.

To align the selected filter indexes across different *constrained* layers, ASSL collects the index vectors of each *constrained* layers and encourages their consistency by maximizing the inner-product of the index vectors, yielding a sparsity structure alignment (SSA) penalty. Alternatively, we follow the same practice by regularizing the weight indexes rather than filter indexes.

Except for the above adaptations, we strictly follow the implementation of ASSL. To sum up, by retaining the key design principles (*i.e.*, filter alignment, SSA regularization, etc.) of ASSL, we deliver an enhanced version of ASSL, which is readily compatible with the off-the-shelf SR network designs in the scenario of weight pruning.

**SRP.** Another representative work of SRP [42] is also dedicated to the pruned filter index alignment considering the residual connection issue. This method selects the indexes

of pruned filters across different *constrained* layers in a random manner prior to the training. Then the selected filters are shrunk by an  $L_2$  regularization with a growing schedule. Typically, the regularization encompasses  $L_2$ -norm of all unimportant filters in the network.

Here, we directly change the pruning units from the filters to the weights throughout the network and follow the same regularization arrangement as SRP. Notably, both of ASSL and SRP are raised upon a pre-trained SR network. In our setting, the pruning is directly conducted upon the network with random initialization.

**N:M Sparsity.** Besides compared methods, another emerging trend of weight pruning is to employ the N:M sparsity [14, 25]. This technology serves as an *hardware-driven standard/regulation* proposed to take advantage of the real-world accelerations upon novel computational platforms (*e.g.*, NVIDIA Ampere GPUs). The proposed method fundamentally different from them by delivering a highly-adaptable solution for the diverse SR network architectures in a *algorithm-motivated perspective*. N:M sparsity is orthogonal to our treatment (see Section 2).

However, to better evaluate the effectiveness of the proposed method, We also compare ISS-P with the the most recent method of SLS [26], which follows N:M sparsity. Note that, this method handles the convolutional networks by customizing the convolutional layers with structural constrains, but not explores and evaluates other types of the neural structures like the Transformer. Therefore, we perform the comparison on the representative convolutional backbone EDSR-L [22].

Specifically, we employ the SLS by pruning the convolutional layers in the residual blocks and the upsampling module. The N:M sparsity is chosen as 2:32 for a pruning ratio of 0.94. We leverage the same training datasets and data prepossessing operations as the settings in Section 4. As compared in Table 6, the proposed method outperforms compared methods including SLS. Considering the orthogonal property, one can easily integrate both trends for a potential hardware acceleration on diverse network designs with weight pruning strategy.

### C. Ablation Study

The behaviour of the pruning methods can be different under different pruning ratios. Therefore, we systematically compare the performances of IHT, ISS-R, and ISS-P under very high pruning ratios (*i.e.*, 0.95 and 0.99). As shown by Tables 7 and 8, ISS-P outperforms the ablated methods at different scales, which is consistent with the results under the ratio of 0.9 (see Table 5). Note that the performance gaps between ISS-P and ablated methods grow as the scale or pruning ratio increases. This is because ISS-P not only better selects the sparse structure, but also retains trainability of the sparse network (see Section E).

| Backbones | Methods         | Set5  |        | Set14 |        | B100  |        | Urban100 |        | Manga109 |        |
|-----------|-----------------|-------|--------|-------|--------|-------|--------|----------|--------|----------|--------|
|           |                 | PSNR  | SSIM   | PSNR  | SSIM   | PSNR  | SSIM   | PSNR     | SSIM   | PSNR     | SSIM   |
| EDSR-L    | scratch         | 29.60 | 0.8522 | 26.35 | 0.7312 | 25.92 | 0.7003 | 23.69    | 0.7303 | 27.28    | 0.8570 |
|           | $L_1$ norm [20] | 29.61 | 0.8526 | 26.36 | 0.7318 | 25.93 | 0.7011 | 23.70    | 0.7313 | 27.35    | 0.8582 |
|           | ASSL [41]       | 29.85 | 0.8568 | 26.54 | 0.7368 | 26.07 | 0.7064 | 24.09    | 0.7461 | 27.93    | 0.8690 |
|           | SRP [42]        | 29.78 | 0.8558 | 26.47 | 0.7349 | 26.02 | 0.7036 | 23.89    | 0.7392 | 27.72    | 0.8656 |
|           | SLS [26]        | 29.76 | 0.8558 | 26.41 | 0.7339 | 25.95 | 0.7029 | 23.76    | 0.7369 | 27.39    | 0.8576 |
|           | ISS-P (ours)    | 30.23 | 0.8628 | 26.74 | 0.7428 | 26.21 | 0.7109 | 24.43    | 0.7596 | 28.51    | 0.8783 |

Table 6. A more comprehensive performance comparison of different methods upon the representative CNN backbone, EDSR-L [22] at the scale of the  $\times 4$ . The method [26] following the N:M sparsity standard is also incorporated. The pruning ratio is 0.95.

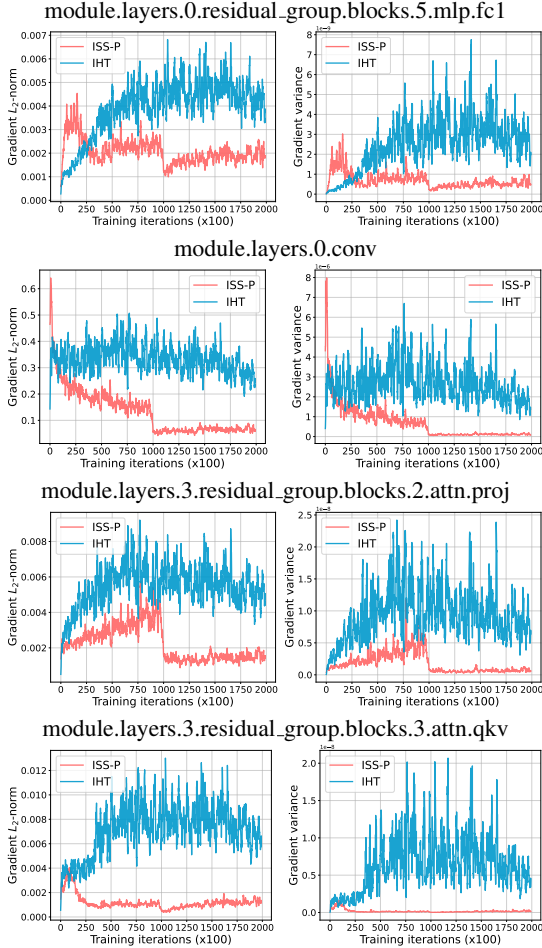


Figure 5. Trainability comparison of ISS-P and IHT. The layer-wise gradient  $L_2$ -norm and variance in the pruning stage ( $1 \times 10^5$  iterations) and the first  $1 \times 10^5$  iterations of fine-tuning stage are plotted. We choose four representative layers, *i.e.*, a fully connected layer (*top*), a convolution (*middle*), a projection layer (*middle*), and a linear layer (*bottom*) from the SwinIR-Lightweight.

## D. Visualization Comparison

In Figs. 7~16, we provide more visualization of different methods under the a very high pruning ratio of 0.99 and scale of  $\times 4$ , which is the most challenging scenario. The proposed performs better by introducing less distortions, especially on high-frequency textured patterns, indicating the

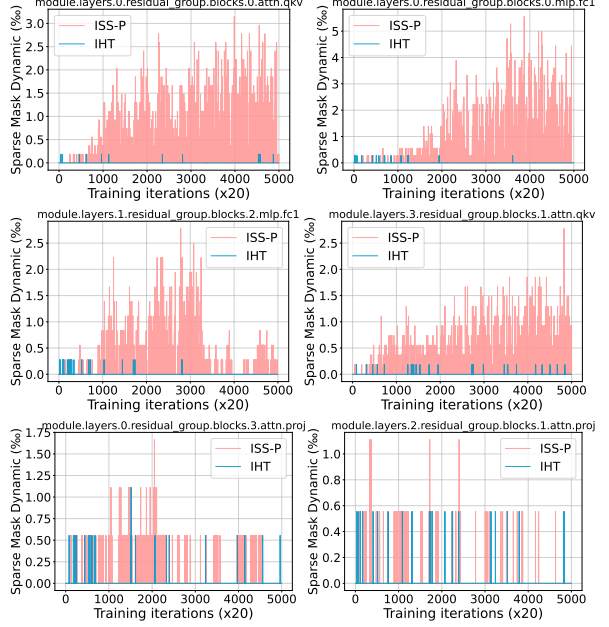


Figure 6. Dynamics of the Sparse structure induced by ISS-P and IHT in the pruning stage. The proposed method, ISS-P, allows a more active sparse pattern exploitation adapting to the optimization. We choose six representative layers (*i.e.*, 1st, 14-th, 3rd, 36-th, 56-th, and 80-th) from the SwinIR-Lightweight backbone [21].

strong modeling capacity of the selected sparse structure.

## E. Model Discussion

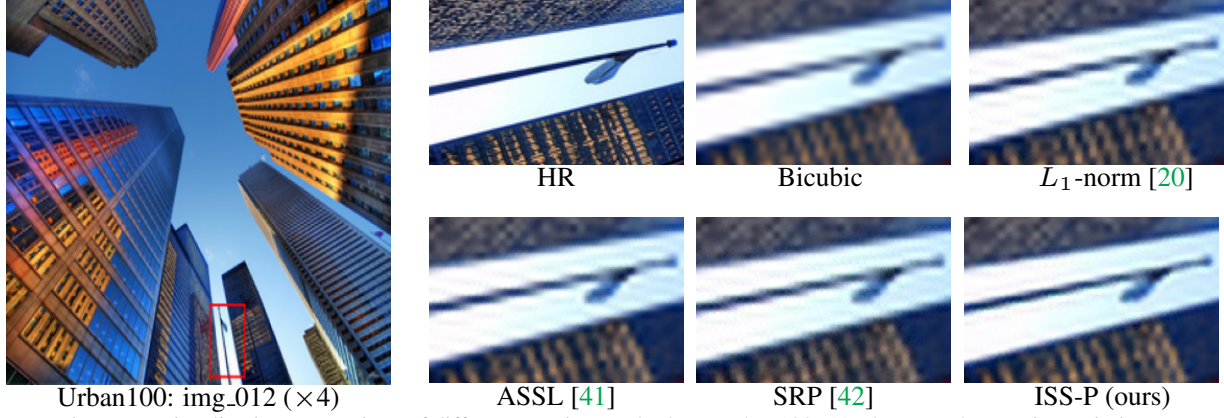
Both the proposed ISS-P and IHT select the unimportant weights per layer in each iteration. Therefore, measuring the number of weights that are categorized into different importance groups between the consecutive iterations helps infer the effect of the pruning methods. In Fig. 6, we provide more visualizations of representative layers in SwinIR-Lightweight. The weight significance flips in ISS-P happens more frequent than that of IHT, which means the proposed method potentially pursues more sparse possibilities in an active manner. We also provide more visualizations of the gradient statistics on different layers in Fig. 5. The gradient  $L_2$ -norm of ISS-P presents a preferred convergence tendency over the IHT regardless of the layer structures, which indicates the promising adaptability of the proposed method across different neural architectures.

| Methods | Scale      | Set5  |        | Set14 |        | B100  |        | Urban100 |        | Manga109 |        |
|---------|------------|-------|--------|-------|--------|-------|--------|----------|--------|----------|--------|
|         |            | PSNR  | SSIM   | PSNR  | SSIM   | PSNR  | SSIM   | PSNR     | SSIM   | PSNR     | SSIM   |
| IHT     | $\times 2$ | 35.17 | 0.9448 | 31.49 | 0.8978 | 30.57 | 0.8781 | 27.95    | 0.8740 | 32.91    | 0.9519 |
| ISS-R   | $\times 2$ | 35.37 | 0.9462 | 31.60 | 0.8983 | 30.66 | 0.8790 | 28.10    | 0.8730 | 33.31    | 0.9543 |
| ISS-P   | $\times 2$ | 35.86 | 0.9496 | 31.89 | 0.9015 | 30.87 | 0.8819 | 28.40    | 0.8777 | 34.09    | 0.9584 |
| IHT     | $\times 3$ | 32.96 | 0.9124 | 29.41 | 0.8247 | 28.44 | 0.7884 | 26.23    | 0.8030 | 30.61    | 0.9158 |
| ISS-R   | $\times 3$ | 32.92 | 0.9122 | 29.38 | 0.8239 | 28.43 | 0.7880 | 26.22    | 0.8027 | 30.57    | 0.9121 |
| ISS-P   | $\times 3$ | 33.28 | 0.9161 | 29.59 | 0.8282 | 28.58 | 0.7919 | 26.55    | 0.8123 | 31.28    | 0.9233 |
| IHT     | $\times 4$ | 30.61 | 0.8661 | 27.57 | 0.7567 | 26.93 | 0.7143 | 24.49    | 0.7258 | 27.49    | 0.8562 |
| ISS-R   | $\times 4$ | 30.69 | 0.8677 | 27.61 | 0.7576 | 26.96 | 0.7151 | 24.52    | 0.7273 | 27.61    | 0.8583 |
| ISS-P   | $\times 4$ | 30.97 | 0.8733 | 27.77 | 0.7619 | 27.05 | 0.7187 | 24.73    | 0.7360 | 28.00    | 0.8669 |

Table 7. Ablation study of different methods under the pruning ratio of 0.95 at different scales.

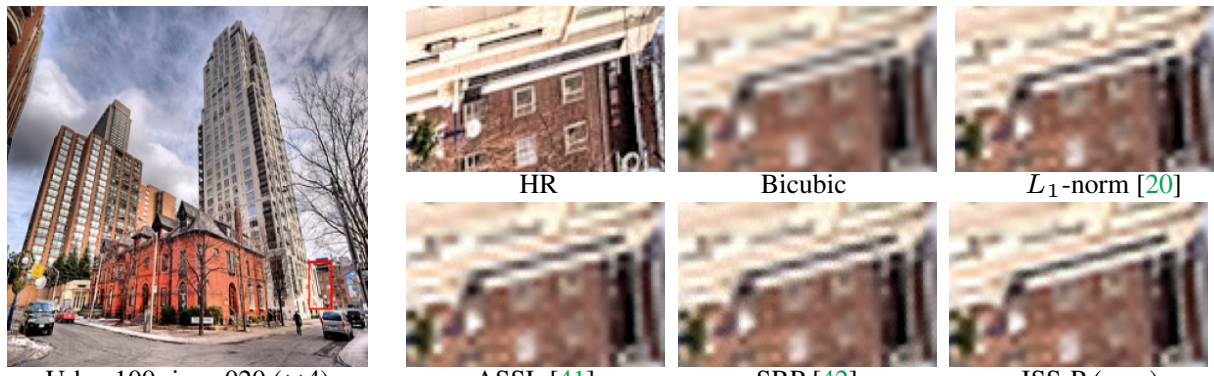
| Methods | Scale      | Set5  |        | Set14 |        | B100  |        | Urban100 |        | Manga109 |        |
|---------|------------|-------|--------|-------|--------|-------|--------|----------|--------|----------|--------|
|         |            | PSNR  | SSIM   | PSNR  | SSIM   | PSNR  | SSIM   | PSNR     | SSIM   | PSNR     | SSIM   |
| IHT     | $\times 2$ | 35.17 | 0.9448 | 31.49 | 0.8978 | 30.57 | 0.8781 | 27.95    | 0.8740 | 32.91    | 0.9519 |
| ISS-R   | $\times 2$ | 35.37 | 0.9462 | 31.60 | 0.8983 | 30.66 | 0.8790 | 28.10    | 0.8730 | 33.31    | 0.9543 |
| ISS-P   | $\times 2$ | 35.86 | 0.9496 | 31.89 | 0.9015 | 30.87 | 0.8819 | 28.39    | 0.8777 | 34.09    | 0.9584 |
| IHT     | $\times 3$ | 31.35 | 0.8853 | 28.35 | 0.8035 | 27.75 | 0.7697 | 25.07    | 0.7630 | 28.03    | 0.8742 |
| ISS-R   | $\times 3$ | 30.94 | 0.8806 | 28.09 | 0.7990 | 27.64 | 0.7660 | 24.92    | 0.7578 | 27.56    | 0.8676 |
| ISS-P   | $\times 3$ | 31.87 | 0.8960 | 28.71 | 0.8102 | 27.98 | 0.7753 | 25.42    | 0.7754 | 28.78    | 0.8889 |
| IHT     | $\times 4$ | 29.13 | 0.8249 | 26.57 | 0.7261 | 26.34 | 0.6916 | 23.57    | 0.6801 | 25.55    | 0.7893 |
| ISS-R   | $\times 4$ | 29.09 | 0.8243 | 26.32 | 0.7260 | 26.32 | 0.6912 | 23.55    | 0.6788 | 25.49    | 0.7977 |
| ISS-P   | $\times 4$ | 29.39 | 0.8331 | 26.73 | 0.7313 | 26.44 | 0.6952 | 23.70    | 0.6873 | 25.81    | 0.8085 |

Table 8. Ablation study of different methods under the pruning ratio of 0.99 at different scales.



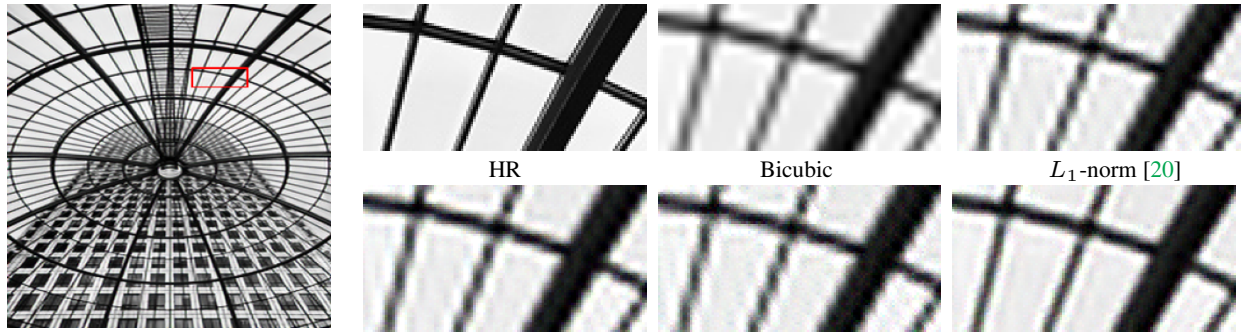
Urban100: img\_012 ( $\times 4$ )

Figure 7. Visualization comparison of different pruning methods on Urban100 [13] dataset. The pruning ratio is 0.99.



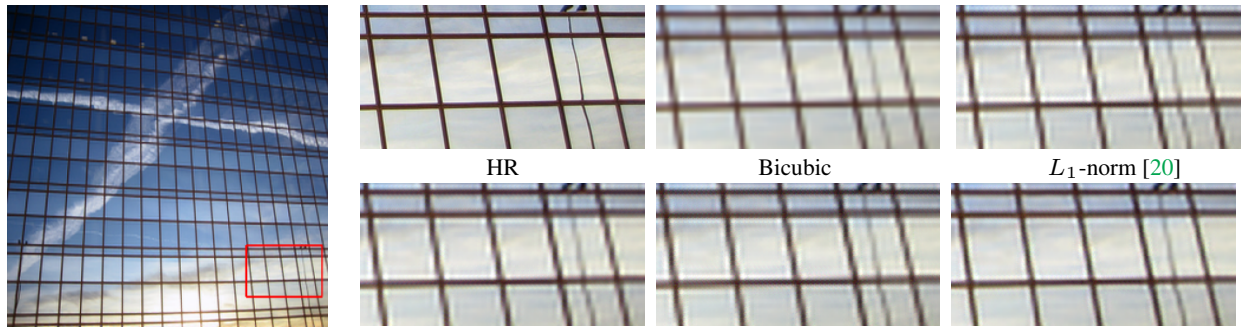
Urban100: img\_020 ( $\times 4$ )

Figure 8. Visualization comparison of different pruning methods on Urban100 [13] dataset. The pruning ratio is 0.99.



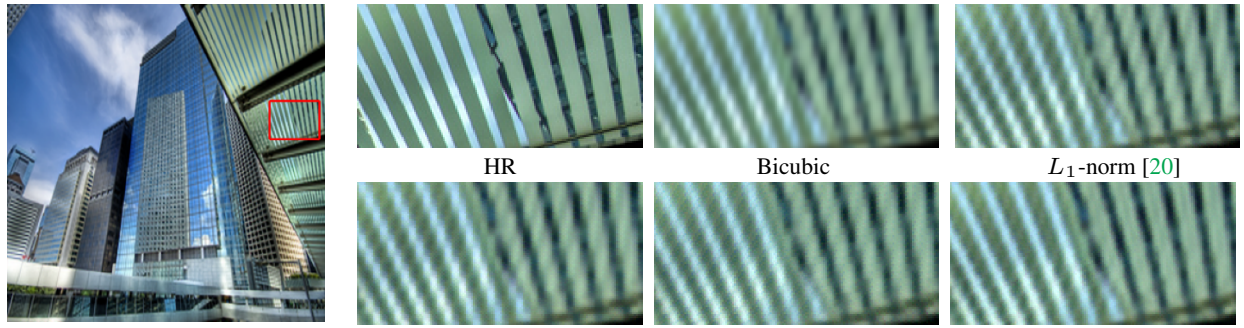
Urban100: img\_072 ( $\times 4$ )

Figure 9. Visualization comparison of different pruning methods on Urban100 [13] dataset. The pruning ratio is 0.99.



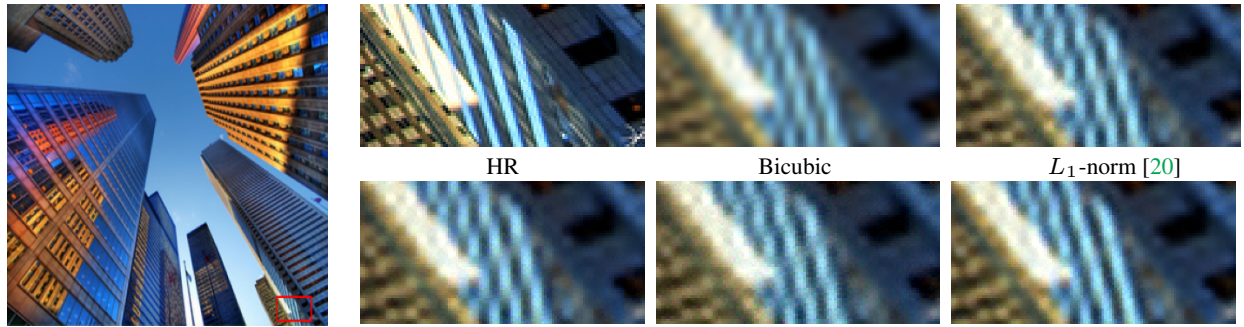
Urban100: img\_055 ( $\times 4$ )

Figure 10. Visualization comparison of different pruning methods on Urban100 [13] dataset. The pruning ratio is 0.99.



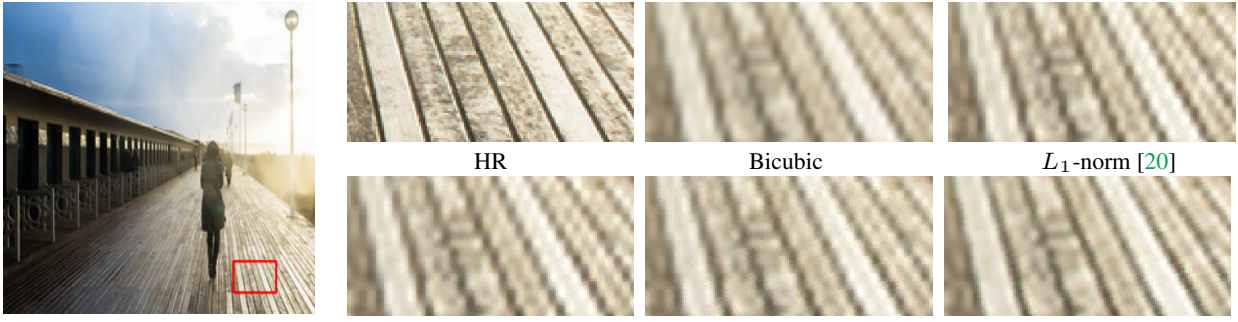
Urban100: img\_061 ( $\times 4$ )

Figure 11. Visualization comparison of different pruning methods on Urban100 [13] dataset. The pruning ratio is 0.99.



Urban100: img\_012 ( $\times 4$ )

Figure 12. Visualization comparison of different pruning methods on Urban100 [13] dataset. The pruning ratio is 0.99.



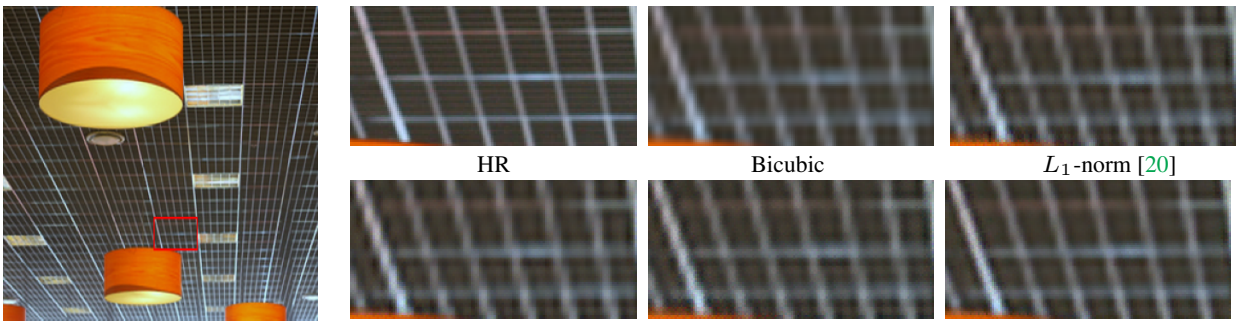
Urban100: img\_032 ( $\times 4$ )

ASSL [41]

Bicubic

$L_1$ -norm [20]

Figure 13. Visualization comparison of different pruning methods on Urban100 [13] dataset. The pruning ratio is 0.99.



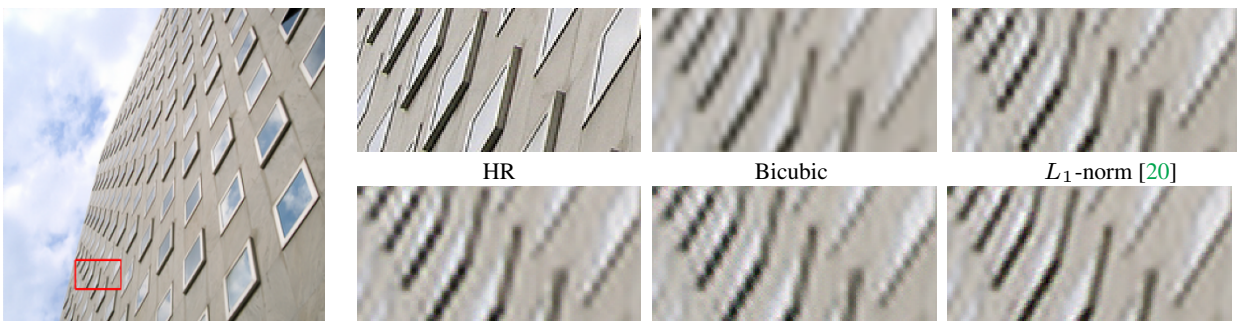
Urban100: img\_044 ( $\times 4$ )

ASSL [41]

Bicubic

$L_1$ -norm [20]

Figure 14. Visualization comparison of different pruning methods on Urban100 [13] dataset. The pruning ratio is 0.99.



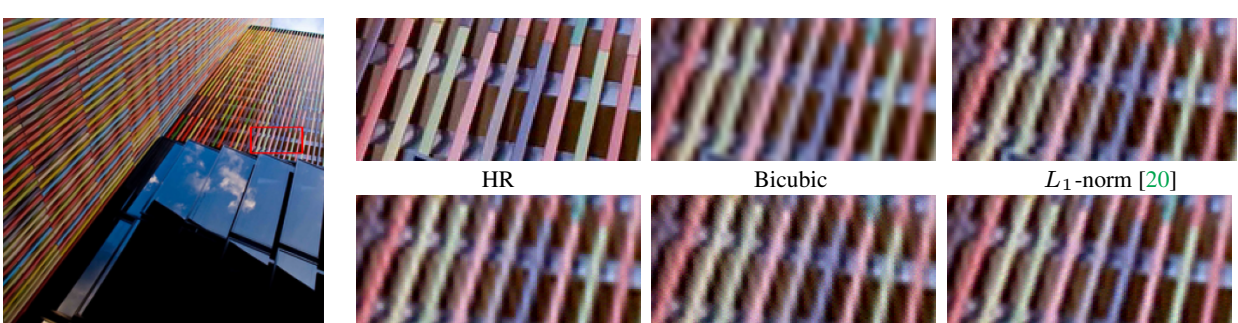
Urban100: img\_010 ( $\times 4$ )

ASSL [41]

Bicubic

$L_1$ -norm [20]

Figure 15. Visualization comparison of different pruning methods on Urban100 [13] dataset. The pruning ratio is 0.99.



Urban100: img\_023 ( $\times 4$ )

ASSL [41]

SRP [42]

$L_1$ -norm [20]

Figure 16. Visualization comparison of different pruning methods on Urban100 [13] dataset. The pruning ratio is 0.99.

## References

[1] Marco Bevilacqua, Aline Roumy, Christine Guillemot, and Marie Line Alberi-Morel. Low-complexity single-image super-resolution based on nonnegative neighbor embedding. 2012. 5

[2] Thomas Blumensath and Mike E Davies. Iterative hard thresholding for compressed sensing. *Applied and computational harmonic analysis*, 27(3):265–274, 2009. 2

[3] Emmanuel J Candès, Justin Romberg, and Terence Tao. Robust uncertainty principles: Exact signal reconstruction from highly incomplete frequency information. *IEEE Transactions on information theory*, 52(2):489–509, 2006. 2, 3

[4] Emmanuel J Candès, Justin K Romberg, and Terence Tao. Stable signal recovery from incomplete and inaccurate measurements. *Communications on Pure and Applied Mathematics*, 59(8):1207–1223, 2006. 2, 3

[5] Chao Dong, Chen Change Loy, Kaiming He, and Xiaoou Tang. Learning a deep convolutional network for image super-resolution. In *Computer Vision–ECCV 2014: 13th European Conference, Zurich, Switzerland, September 6–12, 2014, Proceedings, Part IV 13*, pages 184–199. Springer, 2014. 1, 2

[6] David L Donoho. Compressed sensing. *IEEE Transactions on information theory*, 52(4):1289–1306, 2006. 2, 3

[7] Alexey Dosovitskiy, Lucas Beyer, Alexander Kolesnikov, Dirk Weissenborn, Xiaohua Zhai, Thomas Unterthiner, Mostafa Dehghani, Matthias Minderer, Georg Heigold, Sylvain Gelly, et al. An image is worth 16x16 words: Transformers for image recognition at scale. *arXiv preprint arXiv:2010.11929*, 2020. 2

[8] Song Han, Huizi Mao, and William J Dally. Deep compression: Compressing deep neural networks with pruning, trained quantization and huffman coding. *arXiv preprint arXiv:1510.00149*, 2015. 1

[9] Song Han, Jeff Pool, John Tran, and William Dally. Learning both weights and connections for efficient neural network. *Advances in neural information processing systems*, 28, 2015. 1, 2

[10] Kaiming He, Xiangyu Zhang, Shaoqing Ren, and Jian Sun. Deep residual learning for image recognition. *2016 IEEE Conference on Computer Vision and Pattern Recognition*, pages 770–778, 2016. 2

[11] Yang He, Guoliang Kang, Xuanyi Dong, Yanwei Fu, and Yi Yang. Soft filter pruning for accelerating deep convolutional neural networks. *arXiv preprint arXiv:1808.06866*, 2018. 2

[12] Yihui He, Xiangyu Zhang, and Jian Sun. Channel pruning for accelerating very deep neural networks. In *Proceedings of the IEEE international conference on computer vision*, pages 1389–1397, 2017. 2

[13] Jia-Bin Huang, Abhishek Singh, and Narendra Ahuja. Single image super-resolution from transformed self-exemplars. In *Proceedings of the IEEE conference on computer vision and pattern recognition*, pages 5197–5206, 2015. 5, 7, 11, 12, 13

[14] Itay Hubara, Brian Chmiel, Moshe Island, Ron Banner, Joseph Naor, and Daniel Soudry. Accelerated sparse neural training: A provable and efficient method to find n: m transposable masks. *Advances in Neural Information Processing Systems*, 34:21099–21111, 2021. 2, 9

[15] Justin Johnson, Alexandre Alahi, and Li Fei-Fei. Perceptual losses for real-time style transfer and super-resolution. In *Computer Vision–ECCV 2016: 14th European Conference, Amsterdam, The Netherlands, October 11–14, 2016, Proceedings, Part II 14*, pages 694–711. Springer, 2016. 1

[16] Jiwon Kim, Jung Kwon Lee, and Kyoung Mu Lee. Accurate image super-resolution using very deep convolutional networks. In *Proceedings of the IEEE conference on computer vision and pattern recognition*, pages 1646–1654, 2016. 1, 2

[17] Jiwon Kim, Jung Kwon Lee, and Kyoung Mu Lee. Deeply-recursive convolutional network for image super-resolution. In *Proceedings of the IEEE conference on computer vision and pattern recognition*, pages 1637–1645, 2016. 1

[18] Diederik P Kingma and Jimmy Ba. Adam: A method for stochastic optimization. *arXiv preprint arXiv:1412.6980*, 2014. 5

[19] Vadim Lebedev and Victor Lempitsky. Fast convnets using group-wise brain damage. In *Proceedings of the IEEE conference on computer vision and pattern recognition*, pages 2554–2564, 2016. 2

[20] Hao Li, Asim Kadav, Igor Durdanovic, Hanan Samet, and Hans Peter Graf. Pruning filters for efficient convnets. *arXiv preprint arXiv:1608.08710*, 2016. 1, 2, 3, 5, 6, 7, 8, 10, 11, 12, 13

[21] Jingyun Liang, Jiezhang Cao, Guolei Sun, Kai Zhang, Luc Van Gool, and Radu Timofte. Swinir: Image restoration using swin transformer. In *Proceedings of the IEEE/CVF international conference on computer vision*, pages 1833–1844, 2021. 1, 2, 5, 7, 10

[22] Bee Lim, Sanghyun Son, Heewon Kim, Seungjun Nah, and Kyoung Mu Lee. Enhanced deep residual networks for single image super-resolution. In *Proceedings of the IEEE conference on computer vision and pattern recognition workshops*, pages 136–144, 2017. 1, 2, 5, 8, 9, 10

[23] David Martin, Charless Fowlkes, Doron Tal, and Jitendra Malik. A database of human segmented natural images and its application to evaluating segmentation algorithms and measuring ecological statistics. In *Proceedings Eighth IEEE International Conference on Computer Vision*, pages 416–423. IEEE, 2001. 5

[24] Yusuke Matsui, Kota Ito, Yuji Aramaki, Azuma Fujimoto, Toru Ogawa, Toshihiko Yamasaki, and Kiyoharu Aizawa. Sketch-based manga retrieval using manga109 dataset. *Multimedia Tools and Applications*, 76:21811–21838, 2017. 5

[25] Asit Mishra, Jorge Albericio Latorre, Jeff Pool, Darko Stosic, Dusan Stosic, Ganesh Venkatesh, Chong Yu, and Paulius Micikevicius. Accelerating sparse deep neural networks. *arXiv preprint arXiv:2104.08378*, 2021. 2, 9

[26] Junghun Oh, Heewon Kim, Seungjun Nah, Cheeun Hong, Jonghyun Choi, and Kyoung Mu Lee. Attentive fine-grained structured sparsity for image restoration. In *Proceedings of the IEEE/CVF Conference on Computer Vision and Pattern Recognition*, pages 17673–17682, 2022. 2, 9, 10

[27] Adam Paszke, Sam Gross, Soumith Chintala, Gregory Chanan, Edward Yang, Zachary DeVito, Zeming Lin, Alban Desmaison, Luca Antiga, and Adam Lerer. Automatic differentiation in pytorch. 2017. 5

[28] Russell Reed. Pruning algorithms-a survey. *IEEE transactions on Neural Networks*, 4(5):740–747, 1993. 2

[29] Andrew M Saxe, James L McClelland, and Surya Ganguli. Exact solutions to the nonlinear dynamics of learning in deep linear neural networks. *arXiv preprint arXiv:1312.6120*, 2013. 5, 8

[30] Wenzhe Shi, Jose Caballero, Ferenc Huszár, Johannes Totz, Andrew P Aitken, Rob Bishop, Daniel Rueckert, and Zehan Wang. Real-time single image and video super-resolution using an efficient sub-pixel convolutional neural network. In *Proceedings of the IEEE conference on computer vision and pattern recognition*, pages 1874–1883, 2016. 5

[31] Vivienne Sze, Yu-Hsin Chen, Tien-Ju Yang, and Joel S Emer. Efficient processing of deep neural networks: A tutorial and survey. *Proceedings of the IEEE*, 105(12):2295–2329, 2017. 2

[32] Radu Timofte, Eirikur Agustsson, Luc Van Gool, Ming-Hsuan Yang, and Lei Zhang. Ntire 2017 challenge on single image super-resolution: Methods and results. In *Proceedings of the IEEE conference on computer vision and pattern recognition workshops*, pages 114–125, 2017. 5

[33] Ashish Vaswani, Noam Shazeer, Niki Parmar, Jakob Uszkoreit, Llion Jones, Aidan N Gomez, Łukasz Kaiser, and Illia Polosukhin. Attention is all you need. *Advances in neural information processing systems*, 30, 2017. 2

[34] Huan Wang and Yun Fu. Trainability preserving neural structured pruning. *arXiv preprint arXiv:2207.12534*, 2022. 5

[35] Huan Wang, Can Qin, Yulun Zhang, and Yun Fu. Neural pruning via growing regularization. *arXiv preprint arXiv:2012.09243*, 2020. 4

[36] Zhou Wang, Alan C Bovik, Hamid R Sheikh, and Eero P Simoncelli. Image quality assessment: from error visibility to structural similarity. *IEEE transactions on image processing*, 13(4):600–612, 2004. 5

[37] Wei Wen, Chunpeng Wu, Yandan Wang, Yiran Chen, and Hai Li. Learning structured sparsity in deep neural networks. *Advances in neural information processing systems*, 29, 2016. 2

[38] Syed Waqas Zamir, Aditya Arora, Salman Khan, Munawar Hayat, Fahad Shahbaz Khan, and Ming-Hsuan Yang. Restormer: Efficient transformer for high-resolution image restoration. In *Proceedings of the IEEE/CVF Conference on Computer Vision and Pattern Recognition*, pages 5728–5739, 2022. 1

[39] Roman Zeyde, Michael Elad, and Matan Protter. On single image scale-up using sparse-representations. In *Curves and Surfaces: 7th International Conference, Avignon, France, June 24–30, 2010, Revised Selected Papers 7*, pages 711–730. Springer, 2012. 5

[40] Yulun Zhang, Kunpeng Li, Kai Li, Lichen Wang, Bineng Zhong, and Yun Fu. Image super-resolution using very deep residual channel attention networks. In *Proceedings of the European conference on computer vision*, pages 286–301, 2018. 1, 2

[41] Yulun Zhang, Huan Wang, Can Qin, and Yun Fu. Aligned structured sparsity learning for efficient image super-resolution. *Advances in Neural Information Processing Systems*, 34:2695–2706, 2021. 1, 2, 5, 6, 7, 8, 9, 10, 11, 12, 13

[42] Yulun Zhang, Huan Wang, Can Qin, and Yun Fu. Learning efficient image super-resolution networks via structure-regularized pruning. In *International Conference on Learning Representations*, 2021. 1, 2, 5, 6, 7, 8, 9, 10, 11, 12, 13

[43] Chen Zheng, Yulun Zhang, Jinjin Gu, Yongbing Zhang, Linghe Kong, and Xin Yuan. Cross aggregation transformer for image restoration. *arXiv preprint arXiv:2211.13654*, 2022. 1, 2, 5, 8